12

Cathles, L. M., E. L. Colling, A. Erendi, G. D. Wach, M. W. Hoffman, and P. D. Manhardt, 2003, 3-D flow modeling in complex fault networks: Illustration of new methods with an exploration application in offshore Nigeria, *in* S. Düppenbecker and R. Marzi, eds., Multidimensional basin modeling, AAPG/Datapages Discovery Series No. 7, p. 177–195.

3-D Flow Modeling in Complex Fault Networks: Illustration of New Methods with an Exploration Application in Offshore Nigeria

L. M. Cathles
Cornell University, Ithaca, New York, U.S.A.

E. L. Colling
Texaco Upstream Technology Department, Houston, Texas, U.S.A.

A. Erendi
Cornell University, Ithaca, New York, U.S.A.

G. D. Wach
Texaco Upstream Technology Department, Houston, Texas, U.S.A.

M. W. Hoffman
Texaco Overseas (Nigeria) Petroleum Company Unlimited, Lagos, Nigeria

P. D. Manhardt
GeoGroup Inc., Ithaca, New York, U.S.A.

ABSTRACT

The development of 3-D basin models with complex structural features, fully coupled fluid-flow computations, and network compositional kinetics is just becoming a reality. The new basin models not only reduce exploration risk on a basinwide scale but also prioritize blocks of interest on subbasin or smaller scales. However, the models must be robust and easy to use to be effective in a competitive oil-exploration environment.

In many cases, faults are petroleum migration conduits, especially at depths less than a few kilometers. This is clearly indicated by observations in extensional basins with high deposition rates, such as the Gulf of Mexico and the Niger Delta. Model stability largely involves the handling of faults in 3-D. Most gridding schemes either superimpose a regular grid on complex depositional patterns and structures or capture some or all of the geologic complexity with disjointed grids or grids that are highly deformed in fault zones. A practical alternative to these two extremes is to capture the

geology accurately away from faults and regrid inside faults to avoid grid distortion. This approach allows for easy implementation of a broad set of algorithms for fault permeability, such as controlling permeability by the smear-gouge ratio, when the fault is active or when fluid pressure exceeds a critical level.

The philosophy and essential elements of our approach to modeling 3-D fluid-flow in faults are illustrated with examples from the Gulf of Mexico and then applied in an exploration context in the Niger Delta.

INTRODUCTION

The purpose of a basin modeling study in an area that has already been explored is to further explain the petroleum system and reduce risk of further exploration—especially the risks associated with deeper drilling. The major differences between a frontier exploration model and a nonfrontier exploration model are spatial scale and data intensity. An advantage of higher data intensity is that the models are better calibrated, whereas larger-scale frontier exploration models tend to rely heavily on gross features and basin analogs. Three-dimensional seismic data, structure maps, logs, cores, bottomhole temperatures, pressures, and some maturity data are available in areas such as Eugene Island, offshore Gulf of Mexico, and the "Inner Trend" offshore Niger Delta. The most difficult task is to consistently integrate these data into a petroleum systems model.

This chapter illustrates the modeling approach we will use with example calculations on the Eugene Island area of the Gulf of Mexico (Figure 1). The modeling methods are then applied to address exploration questions in the North Apoi–Funiwa area of the "Inner Trend" offshore Niger Delta (Figure 2). The Eugene Island area is used mainly to illustrate the capabilities of the software we have developed for modeling flow in faults. The Niger Delta is presented as a first application of this software, which we call *Basin*LAB, in a complexly faulted exploration setting.

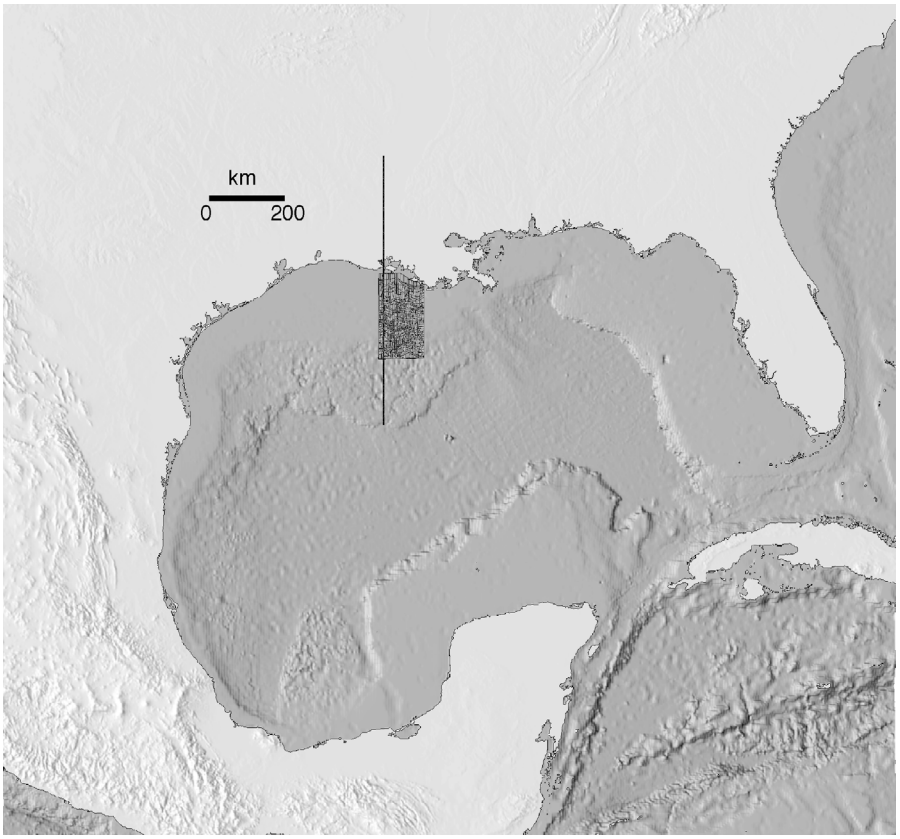

Figure 1. The Gulf of Mexico Basin is a large basin with great remaining exploration potential. The area we modeled is a small part of the offshore Louisiana area marked by dark grid. Cornelius et al. (this volume) modeled salt migration in this gridded area. Shading indicates relief.

OVERVIEW OF THE MODELING CHALLENGE WITH REFERENCE TO THE GULF OF MEXICO

Figure 1 shows the Gulf of Mexico. The dimensions of the small gridded part of the basin are 120 km EW and 230 km NS. According to the *Atlas of Northern Gulf of Mexico Oil and Gas Reservoirs* (Seni, 1997), this area contains ~3.05 billion bbl oil and ~34 tcf gas of partially produced, trapped hydrocarbons. Their distribution is far from uniform: 12% of the oil and 5% of the gas are trapped in South Eugene Block 330 reservoirs, which cover an area that is

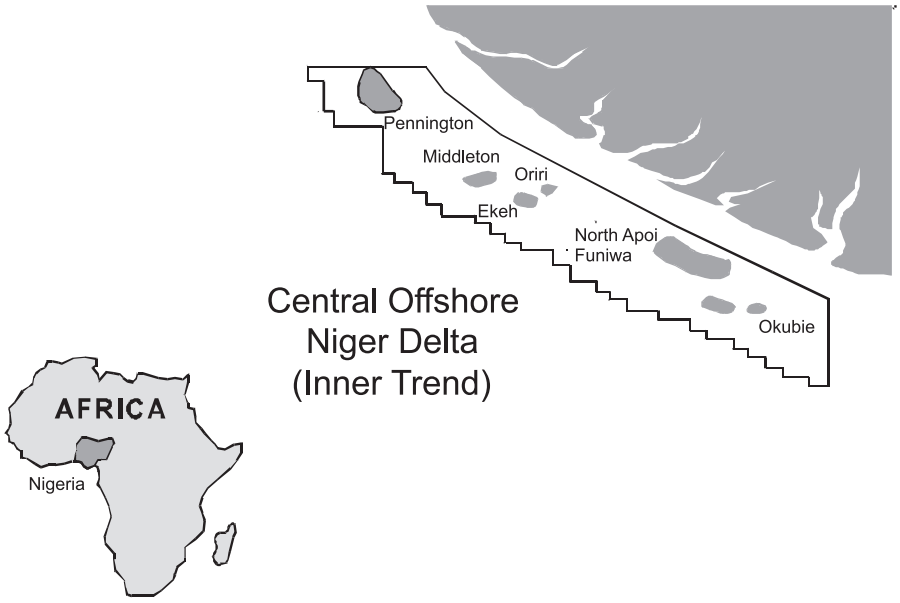

Figure 2. The Niger Delta is located in the Gulf of Guinea. Although the modern delta began in the early Tertiary, the protodelta developed from a series of rift zones associated with the separation of the African and South American continents during the Mesozoic. The North Apoi–Funiwa area is shown in the Inner Trend, which is outlined in black.

less than 0.2% of the total gridded area. Numerous hydrocarbon seeps, which are almost always localized at faults, attest to the fact that the active parts of this basin are very leaky and that the leakage is focused in faults (Roberts and Carney, 1997), at least in the near surface. Probably only a very small fraction of the hydrocarbons that have matured are presently retained in commercially viable reservoirs. We would like to understand in detail how and when hydrocarbons are generated, migrate, and are trapped, and how faults are involved in the process. Because of the spatial and temporal scales involved, this can be accomplished only by modeling the operative processes in three dimensions.

The challenge is substantial. In the Gulf of Mexico, 3-D models— at a minimum— must compute fluid flow on a variety of scales, simulate flow in thin sands and faults, account for permeability changes associated with evolving salt sheets and domes, and properly handle flow in the overpressured zone below the top of overpressure while accommodating any consequences of topography on the top of overpressure surface. This article presents and illustrates our approach to simulating 3-D fluid flow in complexly faulted areas. Cornelius et al. (this volume) discuss and illustrate *Basin*LAB methods for calculating the 3-D history of salt movement and the flow of fluids that results when salt welds develop in the gridded area shown in Figure 1.

THE *Basin*LAB MODELING SYSTEM

As illustrated in Figure 3, *Basin*LAB is composed of three coupled components: a preprocessor called Ageohist that prepares geologic data for finite element modeling; a finite element solver called Akcess.Basin, which calculates temperature, pressure, hydrocarbon maturation, and aqueous and hydrocarbon fluid flow in two or three dimensions; and software associated with DataExplorer, which produces 3-D images of the computational results. In what follows, we describe the first two of these components in enough detail that the basis of the simulations can be understood in general terms. We do not attempt a full mathematical explanation of our computational algorithms in this chapter, although key mathematical concepts are referenced.

The Ageohist preprocessor operates on a personal computer. It receives geologic data as a set of time- or time-depth-converted and -interpreted 2-D sections

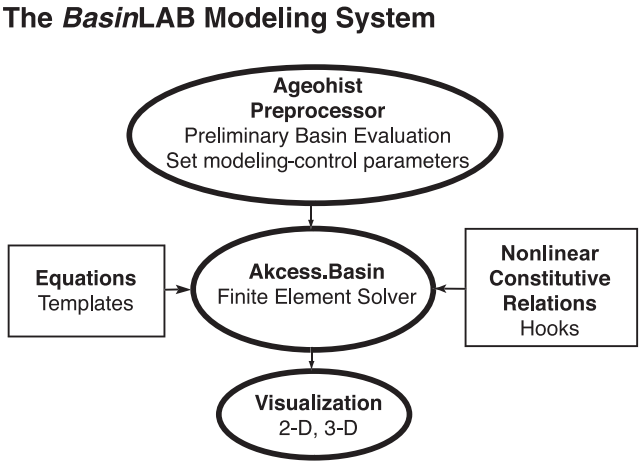

Figure 3. The *Basin*LAB 3-D modeling system is composed of a preprocessor, a finite element solver, and a visualization module.

or as synthetic slices through a 3-D seismic data cube. These sections are linked to produce a 3-D model. The preprocessor now performs several preliminary tasks:

- backstrips and decompacts sediments
- calculates isostatic adjustment in 2-D
- infers salt movement from the sedimentation pattern
- integrates erosion history and paleobathymetry
- calculates the slip across faults
- calibrates the heat flow history, if known, or calculates an inferred heat flow history, if unknown
- calculates a 1-D time temperature history at all nodes that can then be used to calculate vitrinite reflectance (R_o) and assess the total petroleum potential of the basin (pseudo-3-D)

Temperature is later calculated in 3-D and the 3-D thermal history is used to calculate petroleum maturation and migration, but the heat flow history is calibrated with 1-D calculations at the preprocessor stage. This is usually adequate and efficient in terms of work flow. When finished, Ageohist writes a set of ASCII files that defines the evolution of a 3-D finite element grid (effectively a movie of the physical evolution of the basin) and defines the spatial and temporal variation in heat flow.

Akcess.Basin reads the files supplied by Ageohist and uses them to make finite element simulations of the thermal petroleum generation and fluid-flow history of the basin. Akcess.Basin combines a finite element program with (1) a set of templates that defines the temperature and fluid-flow equations to be solved and (2) a set of Fortran subroutines called hooks, which defines at each time-step iteration the nonlinear material and fluid relations required for the solution. Such relations include porosity as a function of lithology and effective stress; thermal conductivity as a function of lithology, temperature, porosity, oil saturation, and gas saturation; and permeability as a function of lithology, porosity, overpressure, and other factors as discussed below. *Basin*LAB has the functionalities listed in Table 1.

Akcess.Basin discretizes space using a Galerkin finite element procedure and uses three Gauss point spatial integration. The finite element algorithm converges transient equations at each time step using a Newton iteration procedure. The forward marching scheme is a Euler one-step process. Details are given in Baker (1983). Heat and fluid mass are conserved in a deforming porous media based on equations derived by Palciauskas and Domenico (1989) and reviewed by Coelho (1997). Boundary conditions specify heat flow with no fluid flow in the base or sides. The water depth and the position of the thermocline in the area being modeled determine the temperature at the sediment-water interface.

Table 1. Phenomena incorporated in *Basin*LAB.

• Sedimentation	• Dynamic top of overpressure
• Compaction	• Heat flow inferred from changes in sediment thickness and/or water depth
• Isostasy	• Heat flow calibration against vitrinite reflectance (R_o)
• Crustal flexure	• Custom R_o kinetics
• Erosion	• Custom petroleum maturation kinetics and stoichiometry
• Salt diapirism	• Water and petroleum migration
• Faulting	• CO_2 generation and titration

Brine flow and petroleum migration are modeled as separate processes. Brine flow is driven by compaction, petroleum maturation, and aquathermal expansion (a comparatively minor contributor). The pressure equation is written in the style first suggested by Gibson (1958) and used by Bredehoeft and Hanshaw (1968). In this formulation, sediment loading increases pore pressure or drives fluid flow depending on the sediment permeability. We have implemented hooks algorithms that increase permeability when a hydrofracture criterion is exceeded. This criterion can be specified on a case-to-case basis but is usually applied when pore pressures reach 0.8 of lithostatic. Until the hydrofracture criterion is met, flow is related to the excess hydrostatic pressure gradient and permeability, as described by Darcy's law.

In the models presented in this chapter, we model the flow of brines only. We assume that in complexly faulted systems, petroleum and brine migrate parallel to each other, at least to first approximation. In the exploration application we present, we are interested in the directions of flow and the proportions of fluid movements through various parts of the system. Therefore, simulation of brine flow alone is adequate to our purposes.

Special features of *Basin*LAB include its ability to predict 3-D salt movements and fluid flow in faults. Our algorithms for salt redistribution assume salt moves in response to differential sediment loading. After subtracting the accommodation space provided by compaction and isostasy (with the flexural rigidity

of the lithosphere taken into account), the remaining depositional space needs are accommodated by moving salt from areas of higher than average to lower than average unaccommodated sedimentation. The methods are described and illustrated in detail in Cornelius and Cathles (this volume).

Faults are handled in Ageohist by the simple expedient of requiring one side of a fault to maintain a fixed distance from the other. The finite element grid is attached to time-stratigraphic horizons on either side of the fault (which provides a very efficient description of the geology), but regridding is allowed in the fault so that element distortion can be minimized. Pasting fault properties onto a finely divided regular grid captures complex fault networks. The advantage of this method is that it allows the permeability of fault elements to be assigned according to any number of simple rules that embody different geologic preferences. Cornelius and Cathles (this volume) describe and illustrate the mechanical aspects of our faulting algorithms. In this chapter, we are concerned with the algorithms that assign permeability to the finite elements within faults.

Before discussing fault permeability, it is important to understand how our model assigned sediment permeabilities. *Basin*LAB sediments are described by their mass fractions of sand, shale, carbonate sand, carbonate mud, and salt. Salt is treated separately and assigned a permeability of 10^{-12} md (e.g., it is impermeable). Other lithologies are assigned permeabilities according to their lithologic mix of fine and coarse fractions and porosity. Sand and carbonate sand are considered coarse sediments, whereas shale and carbonate mud are considered fine. The permeability model is based on measurements and synthetic models of Pennzoil and is illustrated in Figure 4. Essentially, the mix of fine and coarse lithologies establishes the permeability at 20% porosity, and a lithology-dependent porosity dependence is added to this base. The end-member lithologic permeabilities can be freely specified. In Figure 4, shale is assigned a permeability of 10^{-3} md and pure sand a permeability of 10^{2} md. In the models considered in this chapter, the shale permeability is the same but the pure end-member sand permeability is 10 md. Changes in compaction are calculated as a simple function of effective stress and lithology, as shown in the appendix to Cornelius and Cathles (this volume). A shale permeability of 1 μd is not low enough to cause significant overpressuring. Seal elements can be specifically flagged in *Basin*LAB and assigned a very low permeability such as = 10^{-9} md. Flow through salt and seals occurs only when they are hydrofractured.

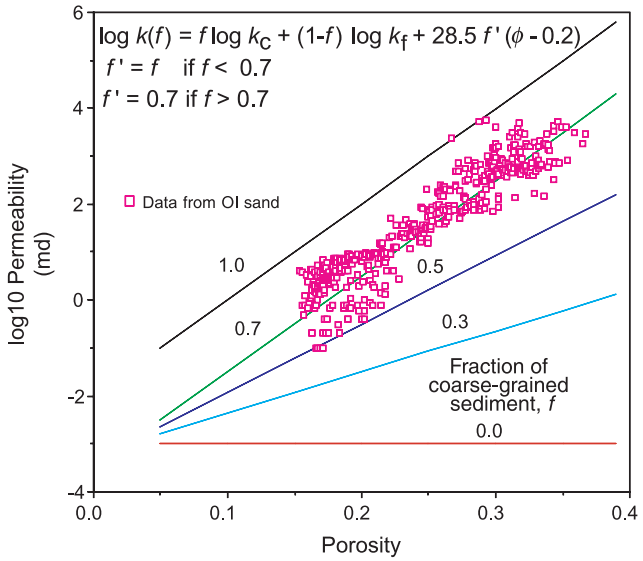

Figure 4. The permeability of sediments is defined in *Basin*LAB as a function of lithology and porosity, as shown in this figure. The red squares are sidewall core permeability measurements from the OI sand, measured and interpreted by Pennzoil. Log k_c is the log permeability (in md) of the coarse-grained end-member lithologies (sand and carbonate sand) linearly combined in proportion to their weight fractions in the sediment. Log k_f is the log permeability similarly defined for the fine-grained lithologic components (shale and carbonate mud). Porosity is ϕ and the fraction of coarse-grained sediment (sand and carbonate sand) is f.

The permeability of fault elements is assigned in a slightly different manner. The two fault permeability algorithms we will use in this chapter are shown in Figure 5. In the first, permeability is assigned according to the sand-shale ratio in the fault gouge. This ratio equals the stratigraphic thickness of sand divided by the sum of this thickness plus the stratigraphic thickness of the shale it has slipped past. Anisotropic fault permeabilities are calculated for fault-parallel and fault-perpendicular flow from the permeabilities of the pure end-member fine and coarse lithologies, as shown in Figure 5. In the second permeability model we will use, the permeability of the fault is related to its slip rate, as shown in Figure 5. The log permeability of a shale (μd) fault is increased in proportion to three times the slip rate (km/Ma). A slip rate of 1 km/m.y. will increase the fault permeability by three orders of magnitude to 1 md.

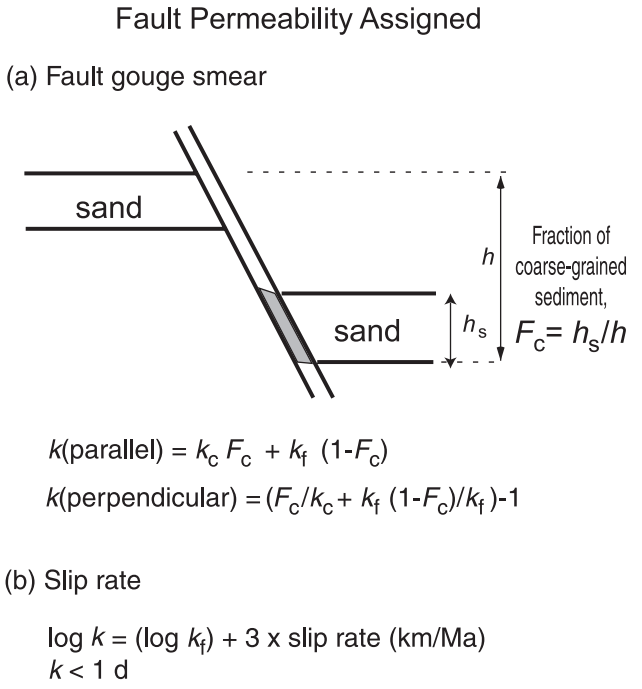

Figure 5. Fault permeabilities are assigned as indicated in this figure in the models presented in this chapter. (a) In the fault gouge smear model, an anisotropic permeability is determined from the ratio of fine- and coarse-grained sediment entrained in the fault. F_c is the fraction of coarse-grained sediment in the fault gouge. Permeabilities parallel and perpendicular to the fault are calculated separately. (b) In the slip rate model, fault permeability is increased in proportion to the rate of slippage across the fault. Permeabilities greater than 1 d are not allowed, according to the sand-shale ratio in fault gouge or according to fault slip rate.

Many models of fault permeability are possible. For example, fault permeability may also be related to fluid overpressure at the base of the fault. At this time, there is no consensus regarding what controls fault permeability of fluid flow in faults, or even whether faults significantly direct subsurface brine and petroleum flow. Our research philosophy is that by developing models that can calculate the consequences of plausible fault permeability dependencies and by analyzing a number of field examples with these models, we will eventually be able to define what controls fluid flow and permeability in faults. This chapter is a step in this process. We first illustrate *Basin*LAB's ability to calculate fluid flow in faults by modeling brine flow in the northeastern border fault of the South Eugene Island Block 330 salt withdrawal minibasin. This fault is known in the area as the ''Red'' or ''A'' fault. We then apply the same methods to a complexly faulted part of the Niger Delta to address questions that arose during exploration in that area.

ILLUSTRATION OF FAULT PERMEABILITY ALGORITHMS IN THE SOUTH EUGENE ISLAND BLOCK 330 AREA OF THE GULF OF MEXICO

Alexander and Flemings (1995) and Alexander and Handschy (1998) describe the evolution of the South Eugene Block 330 minibasin. Figure 6 shows a *Basin*LAB 3-D model of the South Eugene Island minibasin and areas to the north that was constructed by Coelho (1997) by interpreting a Pennzoil 3-D seismic survey. The view is from the north toward the south. The minibasin is on the far (south) side of the model cube. The right face of the cube clearly shows the Red fault.

Figure 7 extracts the sixth section from the cube shown in Figure 6. The section is shaded according to permeability. Shales have a uniform permeability of 1 μd (light gray). Salt (black) has a permeability of 10^{-12} d. For visibility, the Red fault is a uniform dark gray in this illustration, but in most of our models, its permeability varies as a function of depth and time. All the major sands are shown and labeled. By local convention, sands have names that increase alphabetically with depth (e.g., the CA sand is shallower than the EA sand). Sands are shaded according to their permeability (dark is more permeable). The sands are assigned permeability according to their porosity and shale content. Porosity is a major control on permeability, and the sands rapidly decrease in permeability (have lighter shade in Figure 7) with depth as porosity is reduced by compaction.

Both the 3-D model cube and section 6 were backstripped and decompacted to produce 2-D and 3-D models of basin evolution, petroleum maturation, and fluid flow. In this process, the movements on the Red fault were reconstructed over time. This allows us to apply the several algorithms for fault permeability given in Figure 5 and to investigate how different fault permeability relations affect fluid flow.

Brine flow is driven from depth in these models almost entirely by petroleum maturation reactions; compaction is not significant below a depth of about 5 km. Petroleum maturation is calculated in our models assuming a uniform total organic carbon (TOC) content of all shales in the model of 0.4 wt.%. This is typical of shales in the South Eugene Island Area (Holland et al., 1990). Type II Burnham

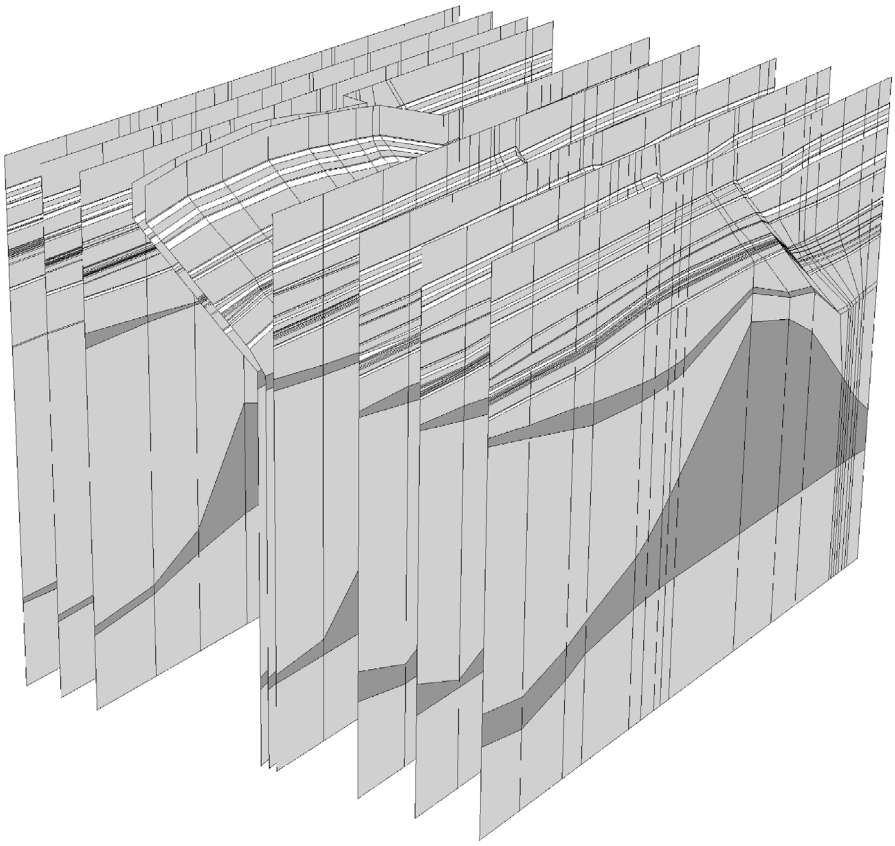

Figure 6. A 3-D model of the South Eugene Block 330 area of the offshore Louisiana Gulf of Mexico is defined by nine 2-D sections. The cube is viewed looking from the north to the south and is about 9 × 12 × 9 km deep. The Block 330 minibasin lies at the far (south) side of the cube. The Red fault is clearly shown on the right face. Sands are white, shales are light gray, and salt is dark gray.

and Sweeney maturation kinetics are assumed and calculated for heat flows calibrated to vitrinite reflectance and bottom-hole temperature data in the Eugene Island Block 330 area (Coelho, 1997). We are, of course, aware that the actual TOC content of the sediments in this area may be quite different, especially in the mid-Cretaceous and Jurassic (Wenger, et al., 1996; Haack et al., personal communication, 1999), but we are interested here only in illustrating fault control on brine migration, and for this purpose, a simple TOC distribution is adequate.

Figure 8 shows how the present-day permeability of the Red fault would change with depth if its permeability was controlled by the fault gouge smear ratio, as specified in Figure 5. Portions of the fault adjacent to sands have permeabilities about twice as large as other parts of the fault in the fault-parallel direction but only slightly higher permeabilities in the fault-perpendicular direction. Overall, the fault-parallel permeability is about 3 md. The fault-perpendicular permeability is little changed from the shale permeability.

Figure 9 shows how the fault-parallel permeability of fault elements initially of sand or shale lithology was modified by fault movement. At the time of deposition (2.27 Ma), the Lentic sand was only slightly compacted (by its own weight) and had a permeability of 10 md. As the fault element containing the Lentic sand was buried, fault slip caused shale to be incorporated and this decreased its permeability. Conversely, the shale that was subsequently deposited in the fault initially had a fault-parallel permeability of 1 μd (10^{-3} md), but its permeability increased as fault movement incorporated sand from the fault walls. The result is that at the present day, both sands and shales in the Red fault have permeabilities near 1 md (see ordinate intersections in Figure 9 and fault-parallel curve in Figure 8).

Figure 10 shows the permeability the Red fault would have as a function of time if slip rate controls fault permeability. The governing relation is given in Figure 5. The fault permeability is isotropic in this model; fault-perpendicular and fault-parallel permeabilities are the same. Figure 10 shows that if slip rate controls fault permeability, the Red fault should have been particularly permeable at about 0.9 Ma.

The pattern of fluid movement is in fact quite different for these two models and different from the pattern that results if the Red fault is given an isotropic 10-md permeability or if the fault is given the permeability of shale (e.g., from a permeability point of view, there is no fault). Flow is from south to north across the Red fault (out of the minibasin) if the permeability of the Red fault is that of shale. This remains largely true if anisotropic permeabilities are specified by the sand-shale smear ratio, except that flow converges on the fault from both the north and south in shallow sands (e.g., in sand units just recently deposited). If the sand-shale smear ratio model is made homogeneous, that is, if the fault-perpendicular permeability is set equal to the

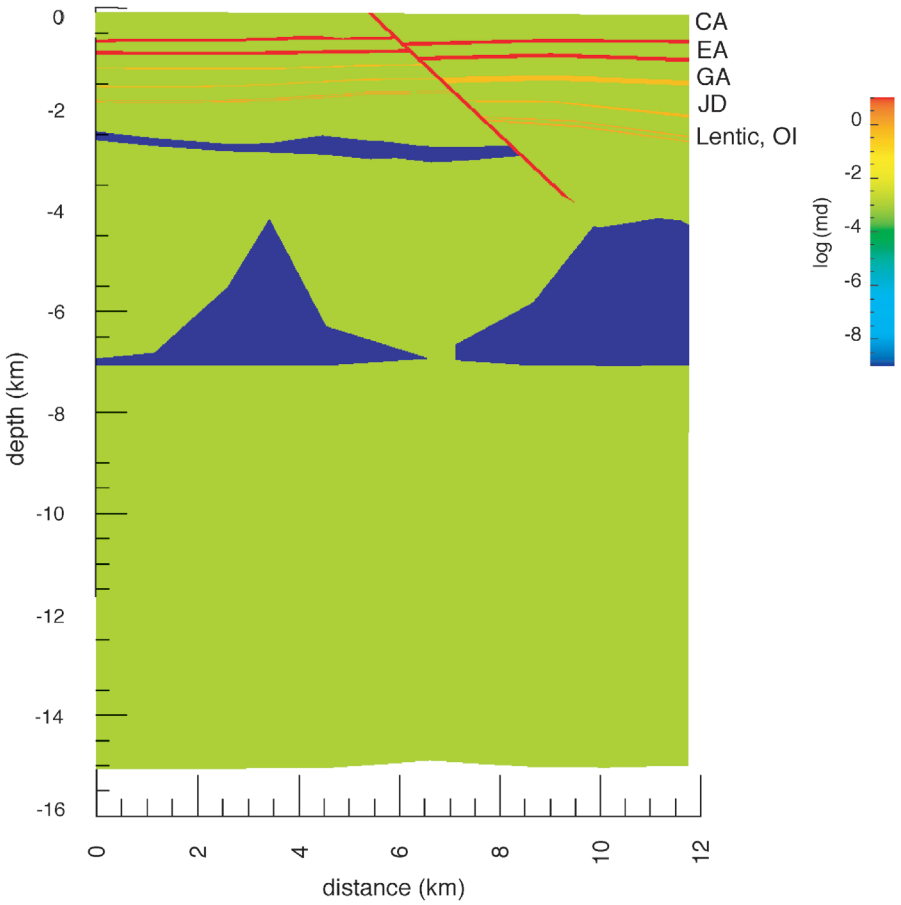

Figure 7. Northeast-southwest section (Line 6) through South Eugene Island data cube (Figure 6). Salt is black, the Red fault is dark gray, and sands are labeled and shaded according to their permeability (dark is more permeable).

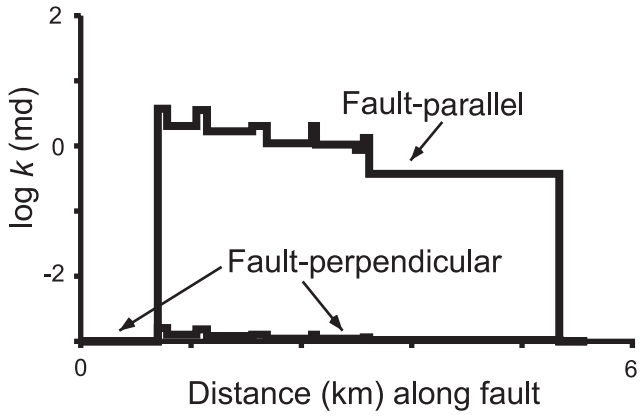

Figure 8. Fault-parallel and fault-perpendicular permeabilities assigned to the Red fault at the present day by the sand-shale fault gouge smear ratio model in Figure 5.

fault-parallel permeability, flow converges on the Red fault from both north and south over most of the basin history, but flow moves across the fault from south to north from 1.7 to 0.9 Ma and from north to south across the fault at 0.65 Ma in the GA sand. At various times (0, 0.54, and 0.9 Ma), flow enters the shallowest sand from the fault and diverges, moving to both the north and the south. For the slip rate model, flow moves across the fault from south to north when the slip is slow, but flow from all sands converges on the fault and moves up it when the slip rate is high. The patterns are thus complex and very dependent on the fault permeability algorithm used. Unfortunately, flow into particular sands is difficult to illustrate and requires being able to zoom in interactively at a visualization workstation.

For the overall pattern of flow, we have found that flow tubes provide the most satisfactory method of visualization. Flow tubes show the trajectory that fluids would take if released at a particular point. Figures 11–13 show the trajectories of flow tubes seeded at the same location for three of the models discussed above. We track flow passing between the deep salt layer and the shallow salt sill because this is the only flow that could carry petroleum. Petroleum is maturing entirely below the shallow salt sill and almost entirely below the lower salt sill. It can be seen from Figures 11–13 that the fault smear and fault slip flow patterns are quite different, and both are very different from the flow pattern that would result if the fault had a uniform permeability of 10 md. Flow crosses the fault from the JD to the Lentic/OI sands in the fault smear model (Figure 11), but crosses the fault only in this location. For the slip rate model, brines cross the fault to enter four hanging-wall sands (Figure 12). Only for the uniform, homogeneous 10-md fault (Figure 13) is there significant discharge through the fault to the seafloor. Flow in the smear ratio model tends to move up through the sands on the footwall (basin) side of the fault, except there is strong flow across the fault in the lowest (Lentic and OI) sands. There is more flow across the fault in the slip rate permeability model and no flow across the fault in the uniform high permeability model.

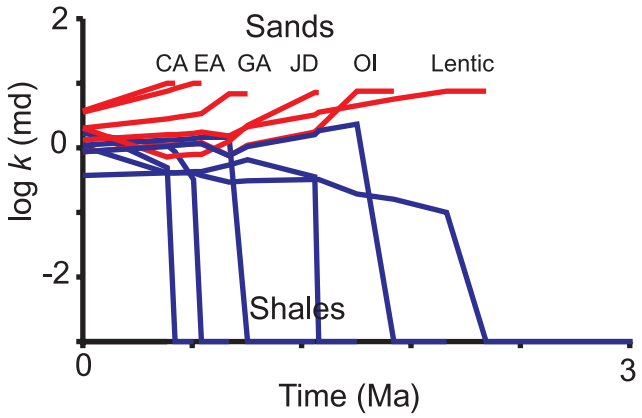

Figure 9. Evolution of fault-parallel permeability in the Red fault according to fault gouge smear model in Figure 5. Compaction and incorporation of shale in elements deposited as sand reduce their permeability, whereas incorporation of sand in elements originally deposited as shale increases their permeability.

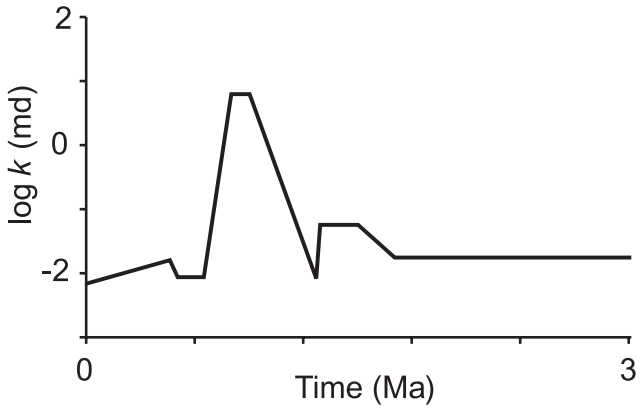

Figure 10. Isotropic permeability of Red fault calculated using fault slip rate permeability model in Figure 5.

Figure 14 shows flow tubes seeded at 9-km depth for the full 3-D Eugene Island model. Anisotropic fault permeabilities are specified by their sand-shale smear ratio. Flow moves around the salt sill, is channeled to a significant degree in faults, and moves horizontally in the shallow sands.

These cases illustrate some of the ways that *Basin*-LAB can simulate flow in faults. It should be emphasized again that we do not know what controls the permeability of faults under geologic conditions. We can probably only hope to determine the important factors by analyzing enough actual examples in enough detail with a variety of fault permeability algorithms. Evidence will come from correctly predicted petroleum distribution and patterns of organic and inorganic chemical alterations. With enough examples, we can hope to gain confidence in permeability algorithms that work. These algorithms can then be applied elsewhere with some confidence.

The first step in this process is reported below. We applied the anisotropic fault smear permeability model to an exploration area in the Niger Delta, and it appeared to work, in the sense that it made "predictions" about petroleum distribution that were compatible with the unusual distribution of petroleum types in the area. These predictions justified a drilling program that successfully intersected oil. We have not carried out 3-D simulations with other fault permeability models. It is possible they would give similar results from an exploration point of view. The methods employed in the Niger Delta are the same as described above for the Gulf of Mexico, except that faulting in the Niger is far more complex. This point should be emphasized because it is by no means clear that flow in very complex fault systems will be affected in the same way as in more insular single faults. A fault-parallel grid similar to the Eugene Island model captured the major listric faults in Nigeria. However, the antithetic faults that connect the main listric faults were captured by the finite element grid in a raster sense. Their permeabilities were assigned using the

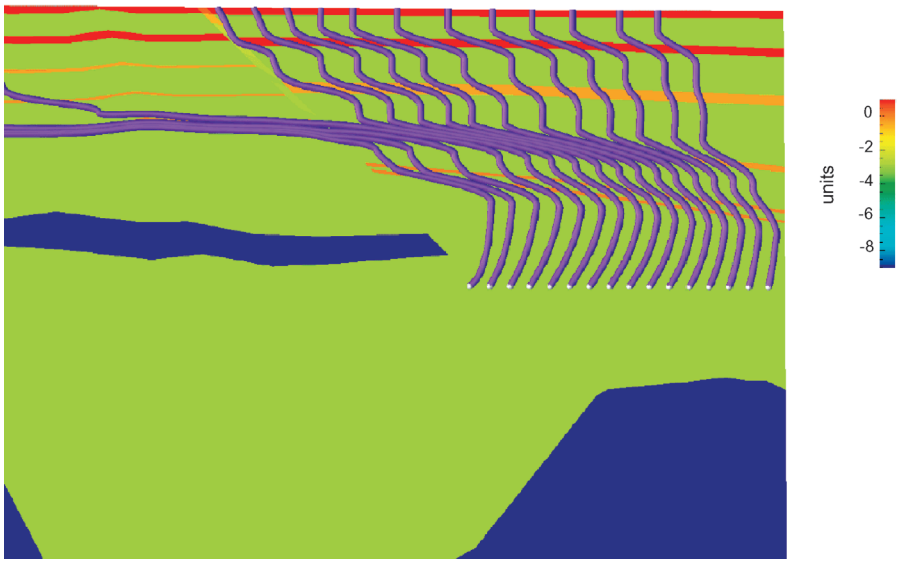

Figure 11. Flow tubes tracking brine flow for simulation with Red fault permeabilities assigned by the anisotropic fault gouge smear model of Figure 5.

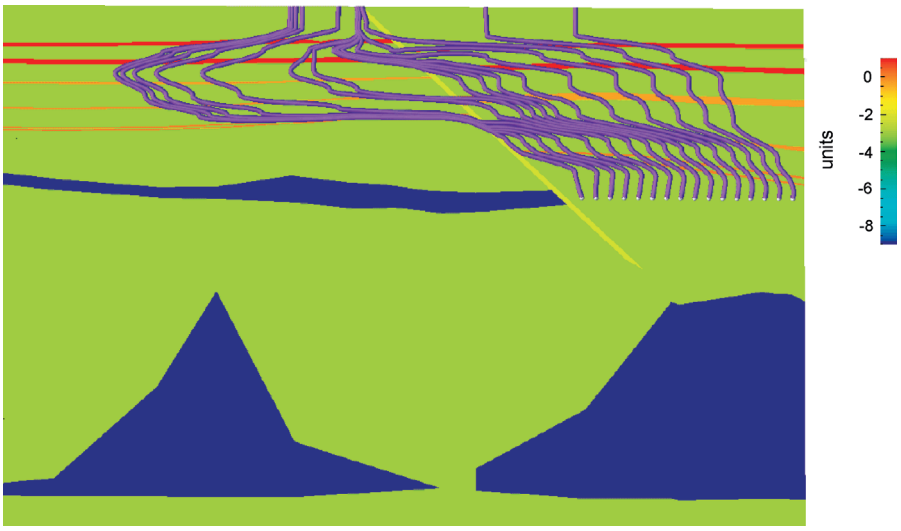

Figure 12. Flow tubes tracking brine flow for simulations with Red fault permeabilities assigned by fault slip rate model of Figure 5.

same methods as described above. The Ageohist grid defines the antithetic faults just as it does the listric ones, so the fault offset and sand-shale smear is known, just as well for the antithetic faults as it was for the listric faults, and the appropriate permeability can be communicated to the (rasterized) finite elements.

OVERVIEW OF NIGER DELTA GEOLOGY

In developing the logic for modeling the North Apoi–Funiwa area, it is useful to review the general geology of the Niger Delta (Weber and Daukoru, 1975; Evamy et al., 1978; Doust and Omatsola, 1990; Wach et al., 1997; Haack et al., personal communication, 1999). The protodelta developed from a series of rift zones associated with the separation of the African and South American continents during the Mesozoic. The modern delta began in the early Tertiary.

The shoreline is constantly modified by wave and tidal processes and is smoothly convex seaward. The gross stratigraphy comprises a prograding package of offlap cycles, with three major time-transgressive lithologic units: the Akata, Agbada, and Benin Formations (Figure 15). The basal Akata Formation is a massive marine shale that is undercompacted, overpressured, and mobile. The overlying Agbada Formation consists of alternating paralic sands and marine shales, which form excellent opportunities for reservoir and top-seal development. The Benin Formation is the latest lithologic unit and is a massive continental sand deposit.

An unusual feature of the Niger Delta is a series of depobelts or depositional cycles that is subparallel to the shoreline (Figure 16), where each depobelt is bounded by a landward growth fault that creates an anticlinal ridge and a seaward counterregional fault. Generally, oil and gas accumulations for the first offshore depobelt (the ''Inner Trend'') are found stratigraphically in the Agbada Formation and structurally in the crestal portions of depobelt subbasins.

Most Niger Delta faulting is caused by extensional deformation. The major exception is the distal section, where toe-thrust faults are common. Extensional faults are normal and generally listric in the form of syndepositional growth faults and crestal tensional relief faults. Relief faults are either synthetic or antithetic, running subparallel to the strike of the subbasins (Figure 17), and synsedimentary

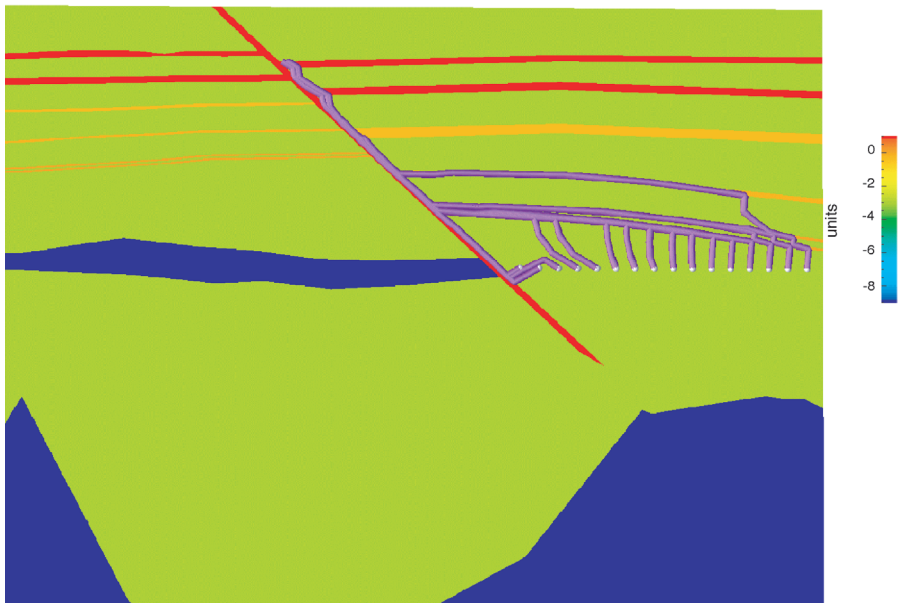

Figure 13. Flow tubes tracking brine flow for simulations with constant 10-md Red fault.

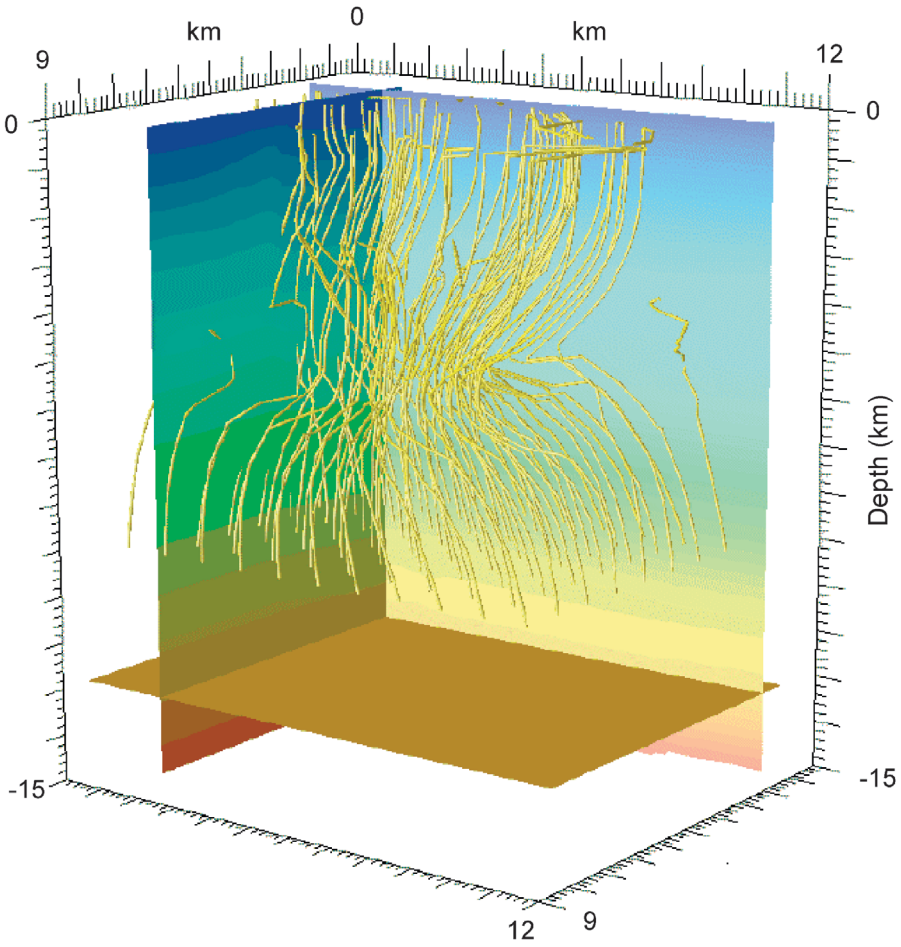

Figure 14. Flow tube tracking brine flow from depth of 9 km in 3-D South Eugene Island Block 330 data cube shown in Figure 6.

faults exhibit growth in the downthrown section, as well as anticlinal (rollover) closures.

STRUCTURE

The North Apoi–Funiwa area (see Figure 19 for location) contains a complex collapsed crest structure with growth faults and antithetic faults. The complexity of the fault system is shown in Figure 18. Growth faults to the northeast are related to growth along the bounding fault that controls structural development in the subbasin. Growth faults to the southwest are younger and in places offset earlier antithetic faults, with less throw. These southwestern growth faults appear to have been conduits for migrating petroleum.

Growth faults generally act as lateral seals, but antithetic faults may or may not seal juxtaposed reservoir strata, depending on fault displacement. A general observation is that the greater the fault displacement, the more likely it is to form a lateral seal.

DEPOSITIONAL ENVIRONMENTS

The Niger Delta is a mixed wave, tide, and fluvial deltaic system (Figure 19). The prograding delta is modified by wave action creating an arcuate coast with beach deposits and back-barrier lagoons. Thick mangroves border the coastline of the lower delta plain. Incised into the coastline are estuaries created by localized subsidence that are infilling with sediment transported by tidal currents during the present-day transgressive to highstand systems tract.

SEQUENCE STRATIGRAPHY

The major sequences were given color codes to avoid confusion with the local lithostratigraphic scheme that crosses sequence boundaries and does not necessarily correlate with the sequence stratigraphic framework (Wach et al., 1997). Sequences were defined based on maximum flooding surfaces (MFS). There are several unconformity-related sequence boundaries, but these are not germane to the modeling objectives

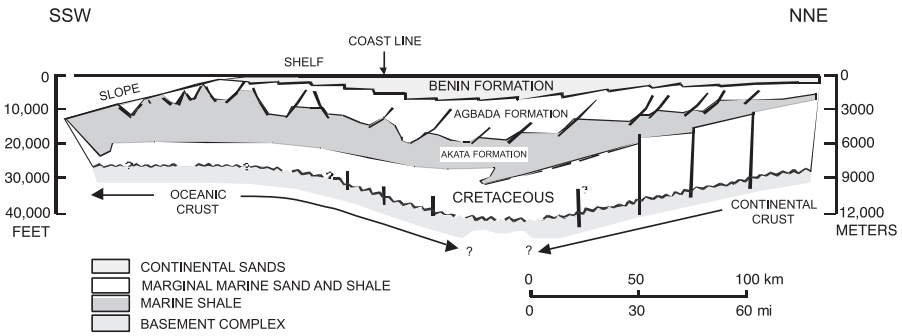

Figure 15. The stratigraphy is a prograding sequence of offlap cycles, with three distinct time transgressive lithologic units: the Akata, Agbada, and Benin Formations. Modified from Whiteman (1982).

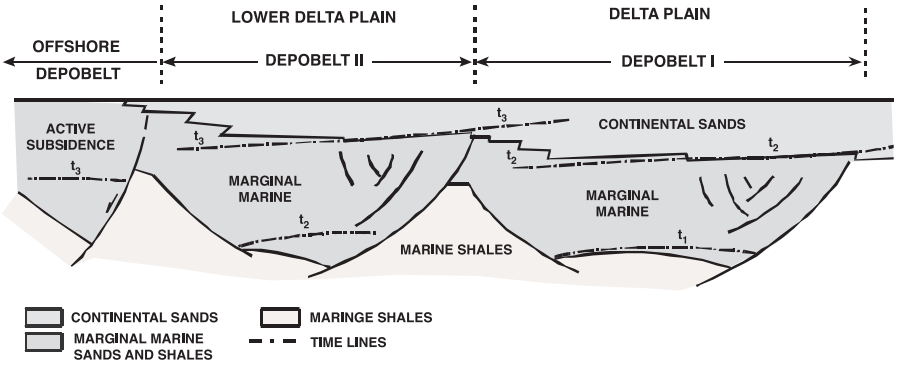

Figure 16. Depobelts are bounded by a major structure-building growth fault to the north and often by a counterregional fault in the basinal direction. Modified from Doust and Omatsola (1990).

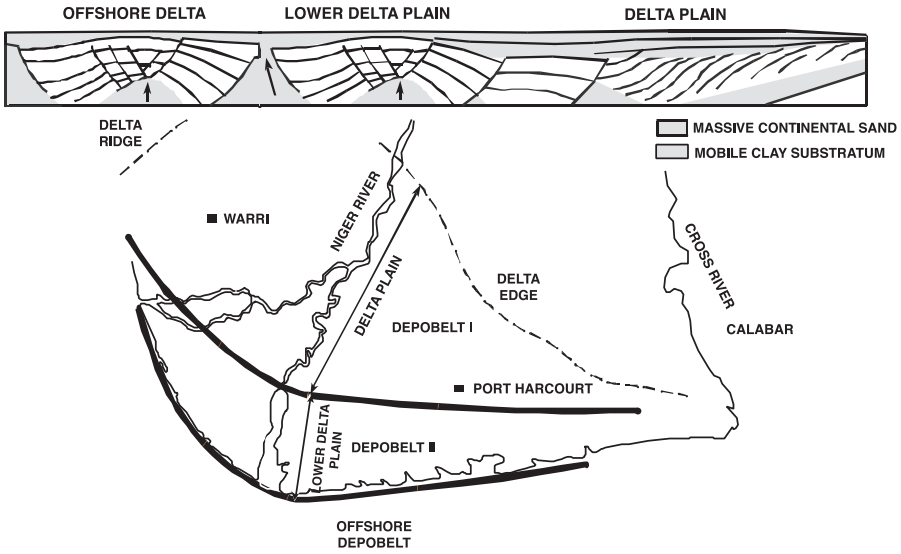

Figure 17. The delta is characterized by a series of depositional cycles (also referred to as depobelts or megastructures), which strike northwest to southeast and run subparallel to the shoreline, defining the Niger Delta subbasins. Modified from Doust and Omatsola (1990).

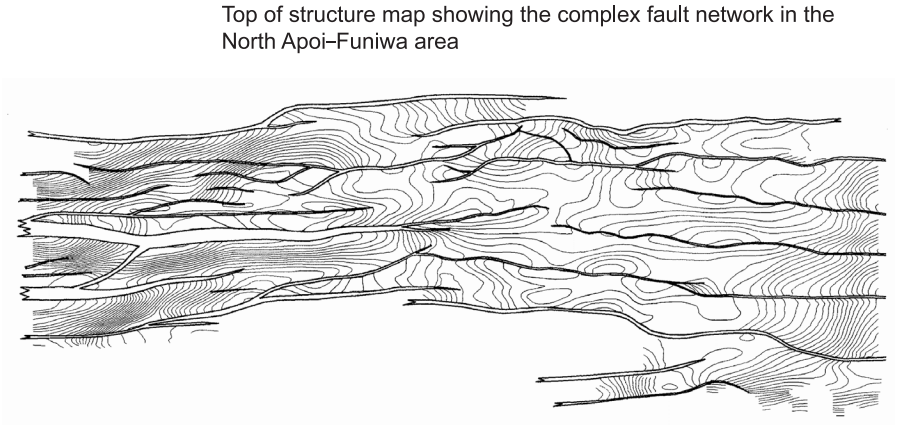

Figure 18. Structure map at the top of the main producing sand within the blue sequence showing the distribution of faults. North Apoi is at the left (northwest) side of the figure and Funawa is on the right (southeast) side. Geographic location is provided in Figure 19. Modified from Wach et al. (1997).

(too detailed), which required age control. Age control is shown on a type log (Figure 20) and is based on abundance peaks of foraminifera, which correlate to interpreted MFS.

The sequences defined by MFS— for drilled and logged sediments below approximately 4000 ft (1219 m) and extending to approximately 13,000 ft (3962 m)— are all in the Agbada Formation and range in age from 3.4 to approximately 10.5 m.y. (middle Pliocene to late Miocene). The blue sequence (Figure 20) contains a thick aggradational section in the middle of the interval, which is interpreted as a locally focused area of deltaic sedimentation resulting in decreased accommodation space. Where the sequences

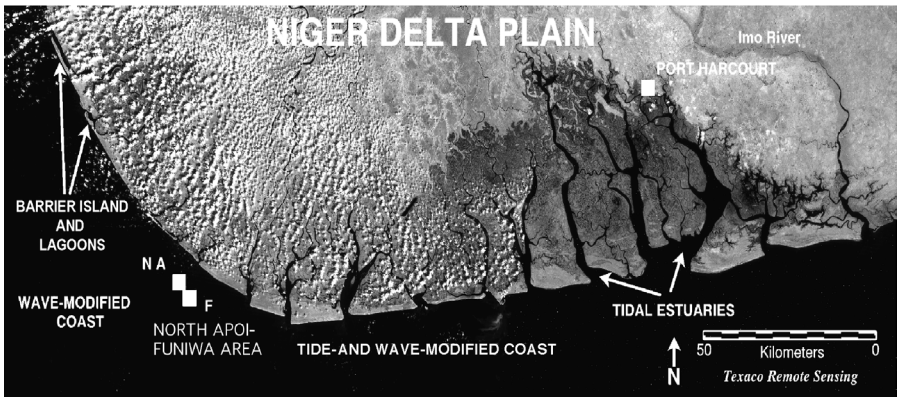

Figure 19. Landsat TM (Thematic Mapper) imager Band 4 mosaic of the Niger Delta illustrating the mixed wave, tide, and fluvial influence on the delta. The environments along the present-day coast of the Niger Delta are apparent in the sediments of the Inner Trend depobelt. Landsat TM Band 4 mosaic details: western scene— path 189, row 57, December 10, 1989; eastern scene— path 188, row 57, December 13, 1984.

are thinner, the delta shifted its focus of sediment transport to other areas along the delta front. The red, yellow, and brown sequences (Figure 20) are thinner, reflecting this shift in delta focus and the resultant increase in accommodation space.

Arrows on the type log (Figure 20) indicate aggradational and progradational sequences. Some of the aggrading lobes appear to turn into prograding lobes basinward. However, this is based on limited well control.

Although data are limited, depositional packages appear to become sandier above the 3.4-m.y. datum. This is probably a response to overall deltaic progradation. More downcutting (possibly channel incision) is apparent on seismic sections updip from the North Apoi–Funiwa area.

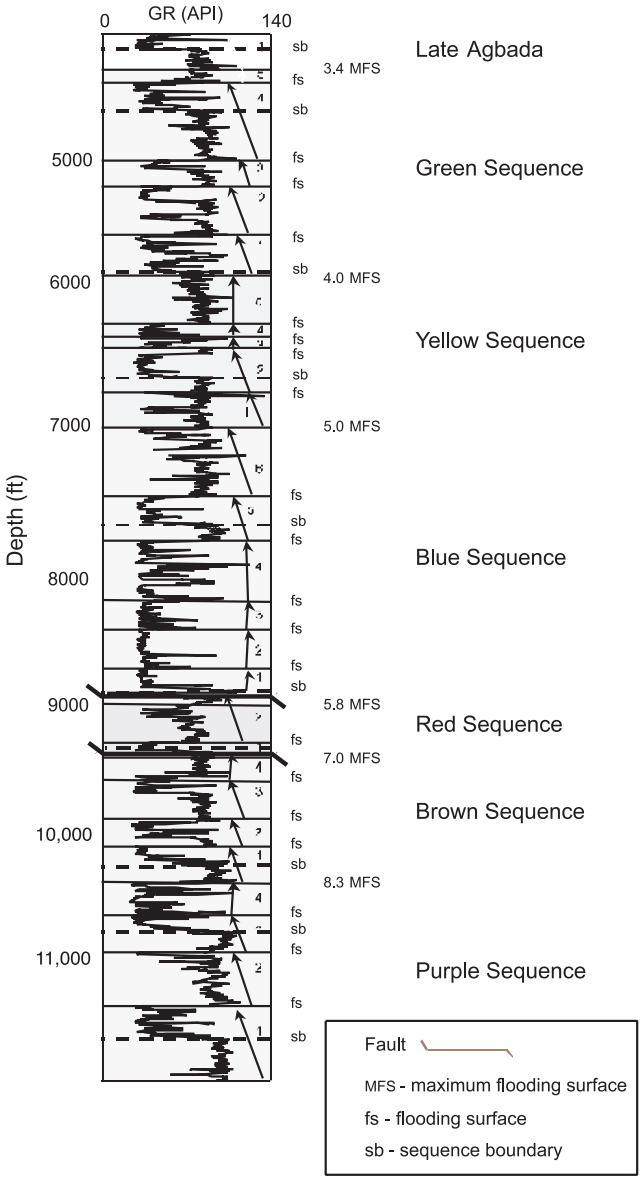

Figure 20. Type section log for the North Apoi–Funiwa field. The age control is based on abundance peaks of foraminifera, correlated to interpreted MFS, which reflect retrogradation phases of the Niger Delta. The sequences are identified by color to avoid confusion with local stratigraphic naming conventions. Modified from Wach et al. (1997).

SOURCE ROCKS AND MATURITY MODELING

Limited seismic resolution and the lack of drill penetrations prevent accurate age assessments of sediments deeper than about 18,000 ft (5486 m) and older than middle Miocene age. However, rough depth and age estimates can be made from seismic data acquired during the early exploration of the Niger Delta shelf. No petroleum source rocks are observed in late Miocene sediments and, considering a similar depositional environment, none is expected in the middle Miocene.

Recently, a Cretaceous marine Type II source rock and an Eocene-mixed marine and terrestrial Type II/III source rock were reported from onshore drilling (Haack et al., personal communication, 1999). These source rocks exhibit strikingly similar age relationships to the Gulf of Mexico source rock system above the Jurassic.

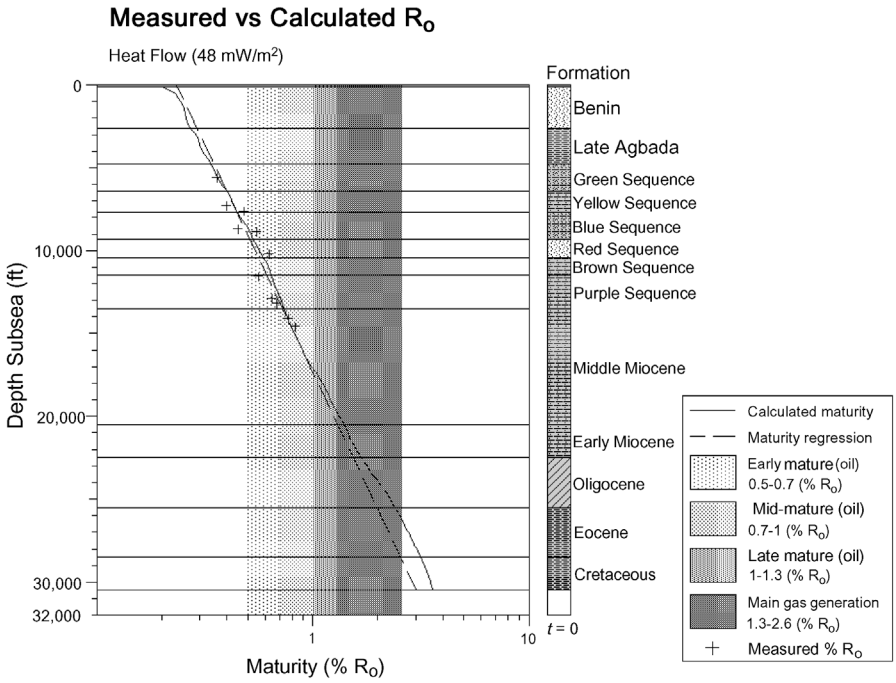

Figure 21. Inner Trend calibration of measured vitrinite reflectance (R_o) with calculated R_o using a heat flow of 48 mW/m^2.

Heat flow and geothermal gradients calibrate very well with measured vitrinite reflectance (R_o). A complicated heat flow or geothermal gradient history is not necessary to match the data. Either a constant heat flow of 48 mW/m^2 (Figure 21) or a geothermal gradient of 1.4°F/100 ft. (25.5°C/km) (Figure 22) is quite satisfactory to match the data. Maturity modeling (Figures 23 and 24)—using Platte River Associates' BasinMod 1-D program and the standard Lawrence Livermore National Laboratories Type II kinetics option—suggests that reservoirs and seals must have been in place and available for petroleum charging by at least the middle Miocene to receive expelled petroleum fluids (Figures 25 and 26). The further implication is that subsequent late Pliocene fault-related migration must be invoked to explain the abundance of shallower oil and gas reservoirs. This suggests that deeper reservoirs charged with petroleum are likely in the middle to early Miocene strata.

FLUID-FLOW MODELING

The purpose of fluid-flow modeling in the North Apoi–Funiwa area was to explain the distribution of petroleum in mostly Pliocene and Pleistocene reservoirs. No model can provide the answer, but models do provide a reasonable explanation that conforms to available data.

The bottom line for 2-D and 3-D fluid-flow modeling for the North Apoi–Funiwa area of the Niger Delta is that modeling does provide an explanation for the petroleum distributions observed. Based on simple 1-D thermal maturity modeling, we know that Pliocene and Pleistocene reservoirs did not exist when the main phase of petroleum generation occurred. Therefore, we must assume that deeper, older reservoirs (probably early to middle Miocene) were present to supply petroleum to the younger reservoirs. This assumption is supported by fault-controlled vertical migration in the petroleum system. Based on growth

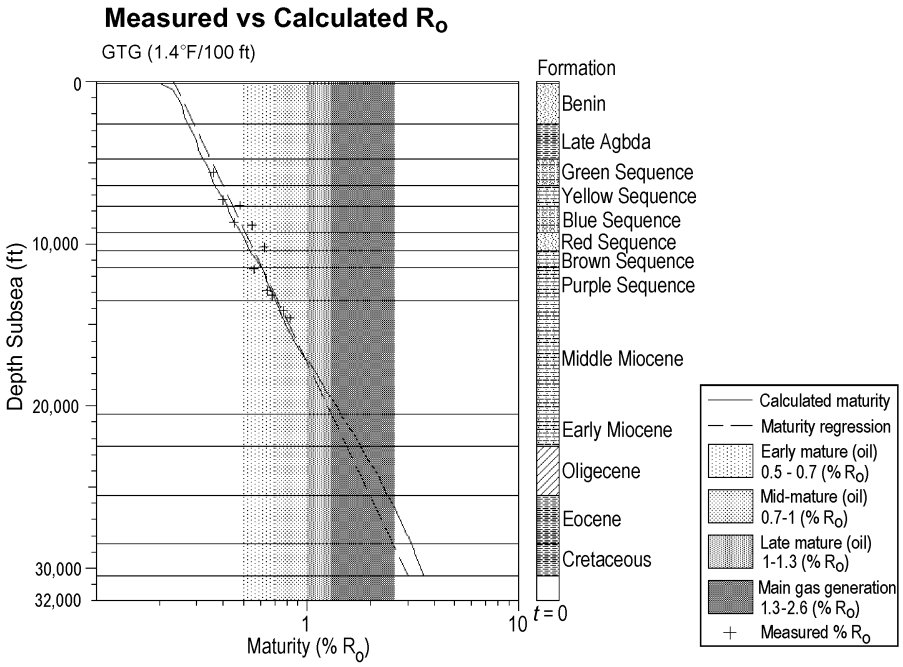

Figure 22. Inner Trend calibration of measured vitrinite reflectance (R_o) with calculated R_o using a geothermal gradient of 1.4°F/100 ft. (25.5°C/km).

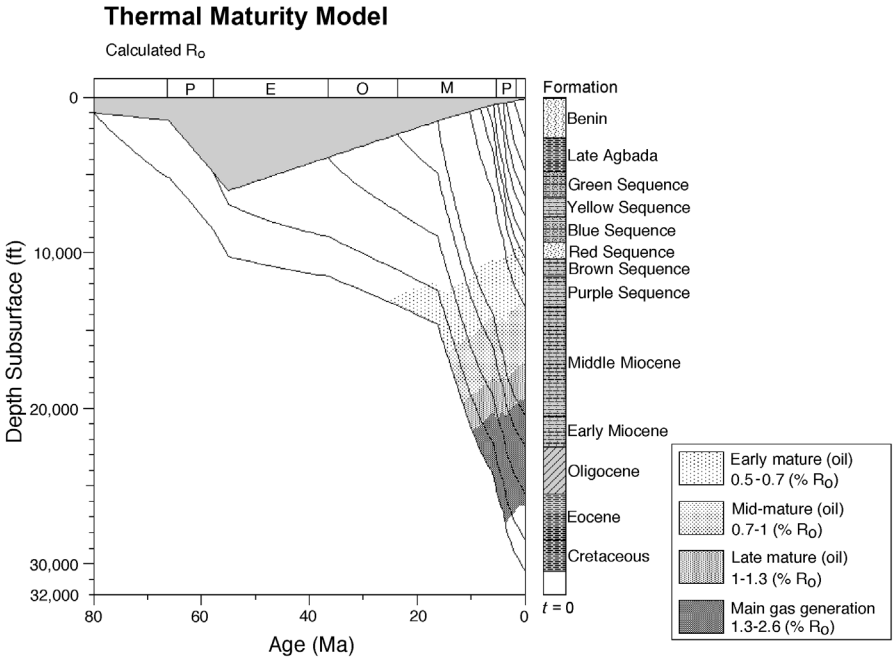

Figure 23. Thermal maturity model based on calculated vitrinite reflectance (R_o).

patterns, it appears that most of the crestal faulting did not begin until about 5–3.4 Ma. This constrains the fluid-flow model to events that could reasonably cause petroleum charging (probably redistribution from older reservoirs) in the North Apoi–Funiwa area to the age range of Pliocene to the present.

2- and 3-D Fluid-flow Models

Initially, we were not able to get the 2-D models to run using *Basin*LAB. Listric and antithetic fault features were far too complicated for a classical finite element Lagrangian grid. To solve this problem, a Eulerian grid was snapped over the Lagrangian grid to maintain complex structural features. A 2-D model of the Funiwa side of the area, where complex antithetic faulting occurs, is shown in Figure 27.

Once the 2-D models were tested, they were linked together to form the 3-D model. Both 2-D and 3-D models showed that the complex fault network is a major controlling factor in the distribution and redistribution of petroleum. The major subbasin listric growth fault acts as a deep carrier system, carrying petroleum from lower Tertiary sediments to the shallower upper Tertiary sediments (early Miocene and younger). Fluid-flow patterns tend to continue in the updip direction by crossing the first (deepest) major antithetic faults encountered and then following the next (seaward-dipping) listric fault toward even shallower sediments. This is shown most clearly in the 2-D fluid-flow cross section on the Funiwa side (Figure 27).

The 3-D models show flow pipes rather than vectors. Essentially, the 3-D graphic (Figure 28) shows that fluids flow updip and make their initial entry into the collapsed crestal structure on the Funiwa side of the North Apoi–Funiwa Field. Once the fluids are in the Pliocene sediments, they tend to migrate upward as well as toward the North Apoi side of the field.

Although the models are not exact, they do make considerable sense as a physically constrained description of the petroleum system. Because the system is

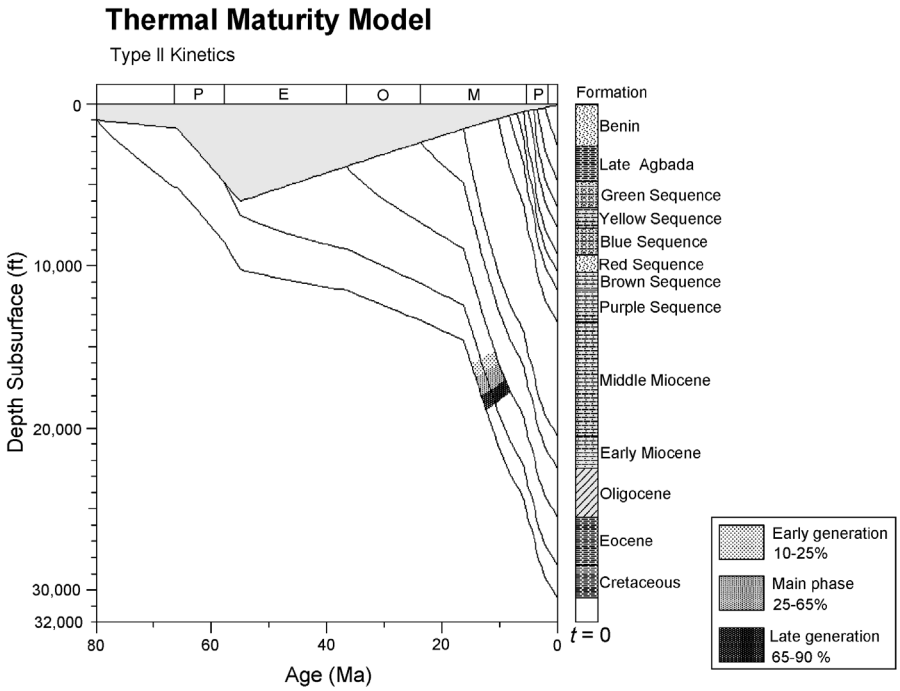

Figure 24. Thermal maturity model of Cretaceous and Eocene source rocks based on Type II kinetics.

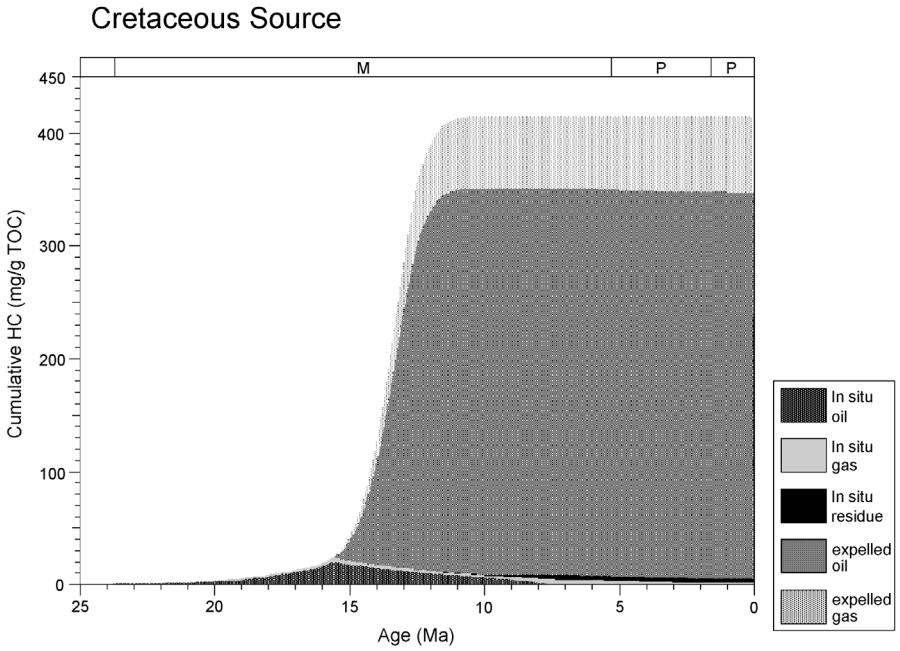

Figure 25. Hydrocarbon generation and expulsion model of Cretaceous source rock based on Type II kinetics.

greatly influenced by vertical migration as well as being exceedingly leaky (in a vertical sense), we can reasonably explain the distribution of petroleum.

Petroleum System Description

Assuming that the source rock is in Cretaceous or Eocene marine shales, the models predict that most of the oil and gas migration occurred by the middle Miocene. Therefore, there must be a reservoir or reservoirs of middle Miocene age or older that trapped this petroleum; otherwise, no petroleum in commercial quantity would exist in the Pliocene-Pleistocene reservoir system. Large Miocene reservoirs are very possible because the depositional system was probably similar to that in the Pliocene period. Moreover, because the sediment load was not as extensive as the Pliocene-Pleistocene, middle Miocene and older sediments were probably in a more classical anticlinal position with less deformation, were less faulted, and were less likely to leak.

As Pliocene sedimentation increased in conjunction with increased basin accommodation space and with deep (Akata) shale deformation, crestal collapse occurred in the rollover anticline. The resulting complex fault structure (a mixture of listric and antithetic faults) brought new migration routes for fluids to move from Miocene and older sediments to the younger Pliocene sediments.

Fluid-flow modeling suggests that petroleum initially flowed up the main listric growth fault (landward side of the subbasin) on the Funiwa side of the North Apoi–Funiwa area. Fluids then crossed over to the seaward listric fault that bounds the seaward edge of the field, using a major antithetic fault as a conduit (most easily seen in Figure 27). Petroleum then moved to shallower levels where it entered the green, yellow, and blue sequence sands. The filled reservoirs spilled progressively through the antithetic fault system toward the landward listric fault.

This fill-and-spill system explains the distribution of oil and gas—both vertically and laterally. In Figures 27 and 28, it is apparent that this is a leaky system and as petroleum moves vertically up the system of sand-shale cycles, petroleum fills to the

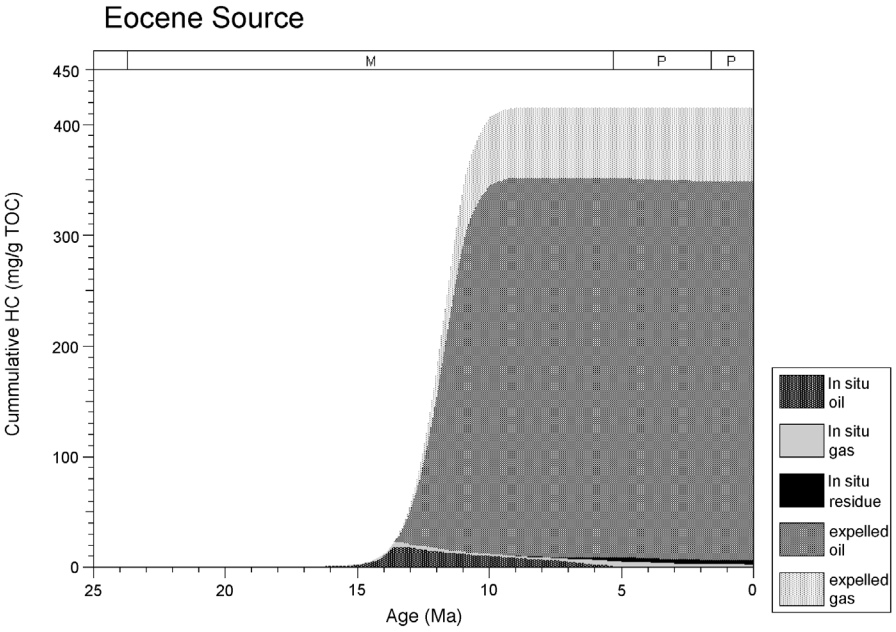

Figure 26. Hydrocarbon generation and expulsion model of Eocene source rock based on Type II kinetics.

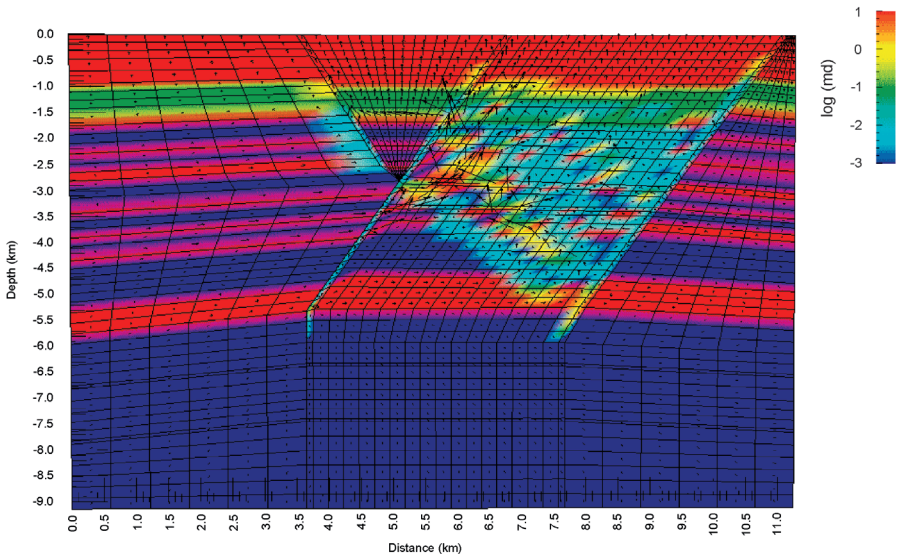

Figure 27. Two-dimensional fluid-flow model in present-day section calculated with the *Basin*LAB basin modeling program. Section runs from southwest on the left (sea side) to northeast on the right (land side). Fluids migrate from a deep reservoir toward the main landward listric growth fault on the Funiwa side of the North Apoi–Funiwa area and cross over to the seaward listric fault by flowing through the first and second antithetic faults. The fluids then move vertically in a diffuse manner. Arrow length indicates relative fluid velocity; shading indicates permeability.

spillpoint. Moreover, as petroleum continues to flow upward from deeper sources, the oil in the deeper reservoirs (upper Miocene and Pliocene) is eventually displaced by gas through the fill-and-spill process. This tends to push oil higher up in the system and explains why we tend to see gas and gas condensate in lower Pliocene to upper Miocene sediments.

The same fill-and-spill process is apparent laterally. Because of the relatively complex system of listric and antithetic faults, oil and gas migrating up the seaward listric fault will fill the first available reservoir that is laterally sealed by a shale as a result of antithetic faulting. As more oil and gas migrate into the same sand, oil will start to spill into the next compartment bounded by yet another antithetic fault. For the Funiwa side of the North Apoi–Funiwa area, this system of reservoir compartments can extend to three or four antithetic faults over (landward) from the seaward listric fault (Figures 29 and 30). This explains the predominance of gas in the first cycle of traps landward of the seaward listric fault.

The above discussion explains the major features of the petroleum system. However, many minor redistributions of petroleum are also occurring (mostly in the vertical sense) because of the leaky nature of the plumbing system.

Exploration Significance of Thermal Maturity and Fluid-flow Modeling

Thermal maturity and kinetic modeling established the timing of petroleum generation as middle Miocene, which indicates that a reservoir or reservoirs of middle Miocene age or older had to exist to receive expelled petroleum from the source rock. Fluid-flow modeling showed that deeper reservoirs (possibly of early to middle Miocene age) will work as a staging area for later leakage into the Pliocene-Pleistocene reservoir system. Extreme overpressuring occurred between 3 and 4 Ma, which suggests this is

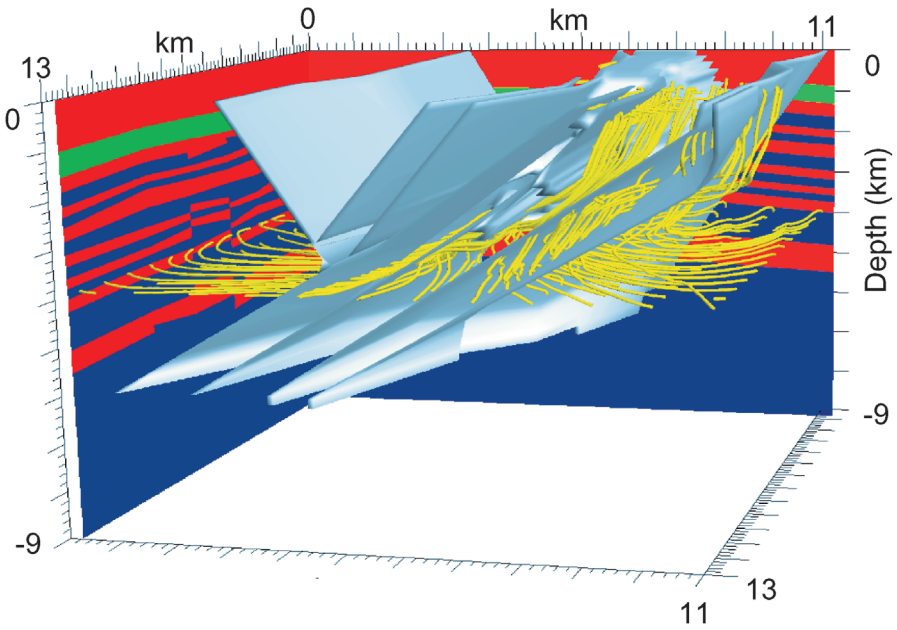

Figure 28. Three-dimensional fluid-flow model using *Basin*LAB showing fault planes' flow pipes at 1.0 Ma, where the near view is on the North Apoi side and the far view is on the Funiwa side of the North Apoi–Funiwa area.

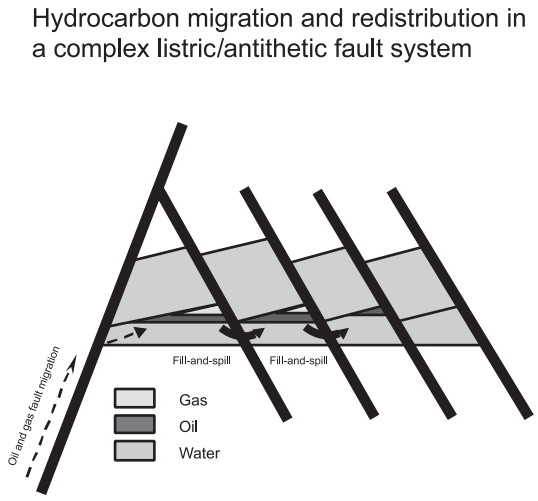

Figure 29. Petroleum that fills reservoirs from the deepest antithetic faults near the seaward listric fault spills progressively vertically and landward. Deep, seaward reservoirs are filled with gas, and landward and higher-level reservoirs are filled with increasingly greater proportions of oil. This figure schematically shows the first stages of filling and spilling. Figure 30 shows later stages.

the most likely age range for a major redistribution of petroleum from deeper reservoirs. Migration from deeper reservoirs can fill the Pliocene-Pleistocene reservoir system with the distribution of oil and gas we observe today. The fact that the flow calculated through the complex system of listric and antithetic faults was immediately compatible with the petroleum-filling scenario that could explain the unusual distribution of petroleum types suggests that fault

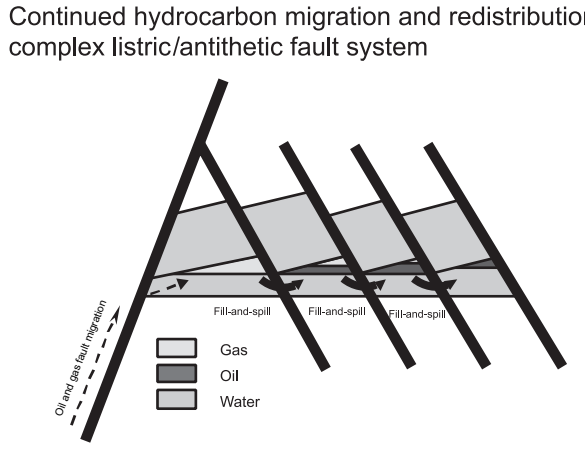

Figure 30. Increasing vertical fill and continued lateral migration of oil and gas, which are migrating under buoyancy drive in a fill-and-spill process within a complex network of listric and antithetic faults. The figure shows reservoir fill at a later stage than Figure 29.

permeabilities may be usefully described by the fault smear model or something close to it. The end-member permeabilities chosen in the modeling are not critical to the results. For example, making pure shale less permeable than 1 μd would not focus flow more to the fault system, because the permeability contrast would still be very large, and this is what counts. The fault permeability dependencies remain of course highly uncertain despite the fact they have been successful in the Nigeria case. What would appear clear from this example is that useful petroleum exploration models will need to explicitly take into account the time- and space-dependent permeability of faults and that modeling in a manner similar to that described here, combined with field studies, could ultimately provide an understanding of how flow in faults affects petroleum migration and accumulation.

ACKNOWLEDGMENTS

The authors would like to thank Texaco Inc., Texaco Overseas (Nigeria) Petroleum Company, Chevron, and the Nigerian National Petroleum Corporation for permission to publish this manuscript. We would also like to thank the corporate sponsors of the Global Basins Research Network for supporting the model development through their corporate affiliate funding and through special projects. The work benefited from insights and data compilation funded by the Gas Research Institute (GRI Grant No. 5097-260-3787). The study was significantly improved by the suggestions and challenges of two reviewers, Domenico Grigo and Andy Pepper, and we thank them for their efforts.

REFERENCES CITED

Alexander, L., and P. Flemings, 1995, Geological evolution of a Pliocene-Pleistocene salt withdrawal mini-basin, South Eugene Island, Block 330, offshore Louisiana: AAPG Bulletin, v. 79, p. 1737–1756.

Alexander, L., and J. Handschy, 1998, Fluid flow in a faulted reservoir system: Fault trap analysis for Block 330 Field, Eugene Island, South Addition, offshore Louisiana: AAPG Bulletin, v. 82, p. 387–411.

Baker, A. J., 1983, Finite element computational fluid mechanics: Washington, D.C., Hemisphere Publishing Co., 510 p.

Bredehoeft, J. D., and B. B. Hanshaw, 1968, On the maintenance of anomalous fluid pressures, I: Thick sedimentary sequences: Geological Society of America Bulletin, v. 79, p. 1097–1106.

Coelho, D. F. S., 1997, Three dimensional analysis of the

temperature field in Block 330, South Eugene Island, Gulf of Mexico: Ph.D. thesis, Cornell University, Ithaca, New York, 292 p.

Doust, H., and E. Omatsola, 1990, Niger delta, *in* J. D. Edwards and P. A. Santogrossi, eds., Divergent/passive margin basins: AAPG Memoir 48, p. 201–238.

Evamy, B. D., J. Haremboure, P. Kamerling, W. A. Knaap, A. Molloy, and P. H. Rowlands, 1978, Hydrocarbon habitat of Tertiary Niger delta: AAPG Bulletin, v. 62, p. 1–39.

Gibson, R. E., 1958, The process of consolidation in a clay with thickness increasing with time: Geotechnique, v. 8, p. 171–182.

Holland, D. S., J. B. Leedy, and D. R. Lammlein, 1990, Eugene Island Block 330 Field— U.S.A., offshore Louisiana, *in* E. A. Beaumont and N. H. Foster, comps., Structural traps III: Tectonic fold and fault traps: AAPG Treatise of petroleum geology: Atlas of oil and gas fields, p. 103–143.

Palciauskas, V. V., and P. A. Domenico, 1989, Fluid pressures in deforming porous rocks: Water Resources Research, v. 25, p. 203–213.

Roberts, H. H., and R. S. Carney, 1997, Evidence of episodic fluid, gas, and sediment venting on the northern Gulf of Mexico continental shelf: Economic Geology, v. 92, p. 863–879.

Seni, S. J., T. A. Tremblay, and D. A. Salazar, 1997, Atlas of northern Gulf of Mexico gas and oil reservoirs: CD-ROM, Bureau of Economic Geology, University of Texas at Austin.

Wach, G. D., M. W. Hoffman, E. L. Colling, O. Ogunyomi, S. Olear, T. L. Fritzel, and P. Russo, 1997, The sedimentology, sequence stratigraphy, and fluid migration history of non-marine and shallow marine reservoirs, North Apoi–Funiwa Field, offshore Niger Delta, *in* K. W. Shanley and B. F. Perkins, eds., Shallow marine and nonmarine reservoirs: Gulf Coast Section Society of Economic Paleontologists and Mineralogists Foundation, 18th Annual Research Conference, p. 365–376.

Weber, K. J., and E. Daukoru, 1975, Petroleum geology of the Niger delta: 9th World Petroleum Congress Proceedings, Tokyo, v. 2, p. 209–221.

Wenger, L. M., A. T. James, K. C. Hood, S. C. Harrison, and O. P. Gross, 1996, Hydrocarbon systems of the northern Gulf of Mexico Basin— Delineation through integration of geochemical and geophysical approaches: AAPG Bulletin, v. 80, no. 8, p. 1344–1345.

Whiteman, A., 1982, Nigeria: Its petroleum geology, resources, and potential: London, Graham and Trotman, 394 p.